AQUA
Water Infrastructure, Ecosystems and Society

corrected Proof

Check for updates

IWA PUBLISHING

AQUA — Water Infrastructure, Ecosystems and Society Vol 00 No 0, 1 doi: 10.2166/aqua.2024.149

Numerical simulation of supercritical flow in sudden contractions flumes

Veli Süme

Department of Civil Engineering, Faculty of Engineering and Architecture, Recep Tayyip Erdogan University, Rize 53100, Türkiye
E-mail: veli.sume@erdogan.edu.tr

VS, 0000-0001-8251-2461

ABSTRACT

In this research, the effect of sudden non-continuous contraction on the energy dissipation of supercritical flows was numerically investigated. This study focuses on energy dissipation in sudden contractions in supercritical flows. The numerical models were studied using FLOW-3D software and the random number generator (RNG) turbulence model. The laboratory tests were performed on sudden contractions of 10–15 cm and used shapes such as geometric trapezoidal and semicircular. Numerical simulations were carried out at a distance of 1.5 m from the supercritical flow generator gate, at a fixed opening of 2.6 cm, with the Froude number in the range of 2.5–7 and the relative contraction in the range of 8.9–9.73. This laboratory study found that as the Froude number of the upstream flow increases, the energy dissipation increases in the upstream ($\Delta E/E_0$) and downstream ($\Delta E/E_1$). For the 15 cm contraction, the results indicated that the energy loss compared with section A is 48.25% and compared with section B, it is 69.5% more than a free hydraulic jump in this channel. According to the conclusion, this value in trapezoidal constriction is 45.73 and 63.6% higher than in free hydraulic jump, respectively.

Key words: energy dissipation, Froude number, pressure, section, simulation model

HIGHLIGHTS

- The Froude number in the range of 2.5–7 and the relative contraction in the range of 8.9–9.73, trapezoidal and semicircular shapes were tested.
- It was observed that as the Froude number increased, energy consumption increased both upstream and downstream.
- According to the hydraulic jump, the energy loss in section A is 48.25% and in section B it is 69.5%.
- The energy loss is 45.73% higher upstream and 63.6% higher downstream than in the free hydraulic jump.

1. INTRODUCTION

The design of channels downstream of hydraulic structures is very important to control hydraulic jumps (Ead & Rajaratnam 2002; Harrison 2015; Abbaszadeh *et al.* 2023; Norouzi *et al.* 2023). Chutes are one of the useful structures to reduce the energy downstream (Chinnarasri & Wongwises 2006). For the first time, the discharge coefficient in these structures was investigated by Hager & Dupraz (1985). Discharge equations for contraction flumes were developed by Samani *et al.* (2021). Results indicated that this function is useful for the design of hydraulic structures. Shock waves are created by the vertical side walls of the chute contract and cause the supercritical flow to deflect. In recent years, many studies have been completed in this field (Molinas 2000; Kaushik *et al.* 2012; Das *et al.* 2014). Hydraulic jumps were investigated in different roughened beds by Hughes & Flack (1984). Trapezoidal wavy beds were investigated by Izadjoo *et al.* (2005). Channels that are often too narrow to reduce the destructive energy of the flow are used and the energy of supercritical flow is higher below the gate. Therefore, solutions must be found to reduce the high flow rate, because high speed causes erosion, foaming, and damage to structures. Parsaie *et al.* (2018) numerically investigated the flow pattern in spillway approach channels. The results show that the current geometry of the left wall causes instability in the flow pattern and makes the secondary and vortex flows at the beginning approach channel. Daneshfaraz *et al.* (2020) investigated numerically and experimentally the effect of sudden narrowing on hydraulic parameters. Yamini *et al.* (2022) investigated the hydraulic performance of the seawater inlet system using computational fluid dynamics (CFD) modeling. The results show that the designer should make every effort to avoid small entrance and filtration areas from the basin to the intake forebay bottom, which could

result in jet outlet and/or supercritical flow. Kyriakopoulos *et al.* (2022) investigated the hydraulic performance of Howell-Bunger and butterfly gates used for downstream outlets in large dams under flood risk. Results showed that based on the numerical study, the parameters of flow patterns, velocity profiles and vectors, turbulence kinetic energy, and formation of flow vorticity were investigated as criteria to determine the appropriate longitudinal distance.

Afaridegan et al. (2023) numerically investigated the hydraulic parameters of modified semi-cylindrical weirs. The analysis of streamline patterns from upstream to downstream of the weirs showed that the curve of the crest provided an opportunity for the flow to harmonize with the surface of the crest.

Al-bedyry *et al.* (2023) investigated the moving hydraulic jump in a trapezoidal channel in a laboratory and showed the connections between discharge and shifting hydraulic jump variables. Parsaie *et al.* (2023) investigated the flow rate coefficient in Samani, Magallanez, Baiamonte, Ferro (SMBF) flumes under free and submerged flow conditions. The results showed that the submerged condition does not reduce the C_d, but it reduces the discharge capacity.

The converging structures that are used downstream of the channels cause the formation of hydraulic jumps. Primary and secondary jump depth changes are among the most important topics in hydraulic engineering. Energy dissipation and the parameters affecting it have been investigated in various types of research.

In recent years, with the development of three-dimensional models and the advancement of computers, it has become possible to extract relationships with the desired accuracy from these models, but three-dimensional models require considerable time to be implemented. Three-dimensional models of flow simulation, including FLOW-3D software, have been widely used in the simulation of flow in open-channel structures. Comparison with experimental results shows that the models in this software can predict flow characteristics with high accuracy. In this model, there are five parental mixing length turbulence models, a kinetic energy equation of turbulence, a two-equation k-ε model, a random number generator (RNG) normalized group model, and a large eddy simulation (LES) model. Therefore, in this research, the hydraulic parameters were investigated using FLOW-3D software. Theoretical equations for the sequential-area and sequential-depth ratios for hydraulic jumps in contraction were developed considering the effects of a contracting width and a sloping bottom. Previous studies show that research conducted in the field of contracting channels has provided effective and useful results. However, further research is needed on the influence of the geometry of the flow path narrowing elements and their arrangement in the channel. Here, the influence of the geometry of the limiting elements of the transverse path of the flow with two semicircular and trapezoidal geometries has been investigated.

2. METHODS

The effective parameters for energy dissipation are listed in the following equation:

$$S = \emptyset(Q, \mathrm{Fr}_0, V, W, B, l, d, D, E_0, E_1, y_0, y_1, y_{\mathrm{cr}}, g, \rho, \mu, L) \tag{1}$$

where S is the amount of energy dissipation, Q is the flow amount, Fr_0 is the Froud number (upstream), V is the flow velocity, W is the width of the channel, B is the width of the constricted section, l is the length of the constriction, d is the opening of the gate, D is the distance between the gate to constriction, E_0 and E_1, respectively, are the specific energy upstream and downstream, y_0 is the initial depth of flow, y_1 is the secondary depth of flow, y_{cr} is the critical depth, L, μ, ρ, and g, respectively, are the length, hydraulic jump, dynamics viscosity, density, and gravitational acceleration. By using the 'Π-Buckingham theorem' and considering the three parameters y_0, g, and ρ as repeated, dimensionless parameters were extracted according to the following equation:

$$\emptyset\left(\mathrm{Fr}_0, \mathrm{Re}_0, \mathrm{Fr}_{\mathrm{d}}, \frac{W}{y_0}, \frac{E_0}{y_0}, \frac{E_1}{y_0}, \frac{l}{y_0}, \frac{B}{y_0}, \frac{d}{y_0}, \frac{D}{y_0}, \frac{y_{\mathrm{cr}}}{y_0}, \frac{L}{y_0}, \frac{y_1}{y_0}\right) = 0 \tag{2}$$

where Fr_0 is the upstream Froude number, Fr_{d} is the downstream Froude number, and Re_0 is the Reynolds number. To make the parameters meaningful, by dividing some of them by each other, the dimensionless parameters are presented in the form of the following equation:

$$\emptyset\left(\mathrm{Fr}_0, \mathrm{Re}_0, \mathrm{Fr}_{\mathrm{d}}, \frac{B}{W}, \frac{E_0}{y_0}, \frac{E_1}{y_0}, \frac{L}{l}, \frac{D}{d}, \frac{y_{\mathrm{cr}}}{y_0}, \frac{y_1}{y_0}\right) = 0 \tag{3}$$

In this research, due to the turbulent nature of the flow, the Reynolds number, as well as the parameters of channel width, constriction length, and gate opening as well as relative jump length, relative critical depth, and relative contraction are neglected. Therefore, the dimensionless relative energy dissipation parameter in terms of independent dimensionless parameters was:

$$\frac{\Delta E}{E_A}, \frac{\Delta E}{E_B}, \mathrm{Fr_d}, \frac{y_1}{y_0} = \phi\left(\mathrm{Fr_0}, \frac{B}{W}\right) \tag{4}$$

where $\Delta E/E_A$ and $\Delta E/E_B$ are upstream and downstream relative energy dissipation, respectively. On the other hand, $\mathrm{Fr_d}$ is the downstream Froude number and y_1/y_0 is the downstream relative depth.

2.1. Numerical modeling

This study investigated the energy dissipation in crescent constrictions in the face of supercritical flow in free jump and submerged conditions over the Froude number range of 2.8–5.7. The higher the Froude number, the higher the energy. The software FLOW-3D was used. Validation of the numerical data of the present research with the laboratory data of Daneshfraz *et al.*'s (2018) research shows that the data are in good agreement with each other. A view of the laboratory flume plan is given in Figure 1(a).

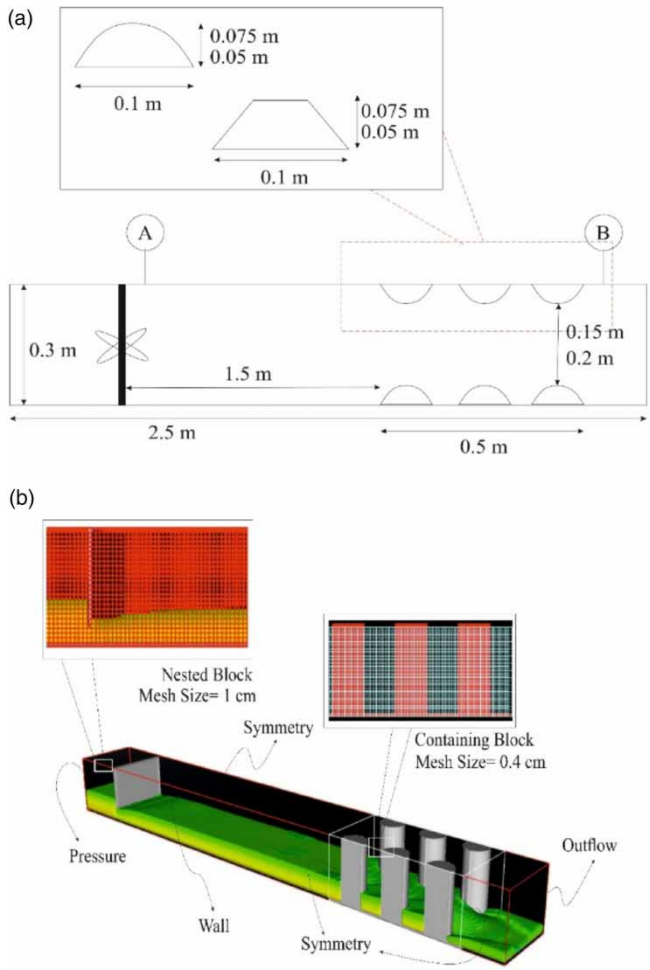

Figure 1 | (a) Schematic image of the current research model; (b) meshing, boundary conditions, and solution field grid.

The optimal cell was selected by performing a simulation on four models with different cell dimensions. Statistical indicators were used to compare the energy dissipation between experimental and numerical results. The statistical indicators are listed here:

$$\mathrm{AE} = \left| \left(\frac{\Delta E_{\mathrm{AB}}}{E_{\mathrm{A}}} \right) \left(\frac{\Delta E_{\mathrm{AB}}}{E_{\mathrm{A}}} \right)_{\mathrm{num}_{\mathrm{exp}}} \| \right| \tag{5}$$

$$\mathrm{RE} = \left| \frac{\mathrm{AE}}{(\Delta E_{\mathrm{AB}}/E_{\mathrm{A}})} \right| \tag{6}$$

$$\mathrm{RMSE} = \sqrt{\frac{\sum_{i=1}^{n} (\mathrm{AE})_i^2}{n}} \tag{7}$$

In the above relationships, ΔE is the energy loss between sections A and B in meters. E_{A} is the flow energy in section A in meters, n: is the number of datapoints, and Equations (5)–(7) are used to calculate absolute mistake, relative mistake, and root mean square mistake, respectively. The results are provided in Table 1.

The results showed that the reduction in the size of the meshes has reduced error. Because the error rates of rows 3 and 4 are almost the same, so row 3 was used to increase the speed of the numerical models. Mesh sizes are between 0.05 and 0.032 m and usually the number of meshes is taken as 3. In this study, two mesh blocks were used. Figure 1(b) shows the boundary conditions and networks in this study. In mesh block 1, the pressure boundary condition for X_{min}, outflow for X_{max}, wall for Y_{min}, Y_{max}, and Z_{min} and symmetry for Z_{max} was used, and in mesh block 2, the symmetry boundary condition for X_{min} and X_{max}, wall for Y_{min}, Y_{max}, and Z_{min} and symmetry for Z_{max} was used.

The FLOW-3D model is one of the most powerful softwares available for solving hydraulic problems; it is based on CFD and can simulate different flows. The governing equations for fluid flow in this software are mass conservation and the Navier–Stokes equations. This model solves the equations with the finite volume method on a gridded field to analyze the incompressible flow and track the fluid interface in Equation (8). The general form of the continuum and the Navier–Stokes equations are given in Equation (9). In Equations (8) and (9), the fluid is considered incompressible.

$$\frac{\partial A}{\partial t} + V\frac{\partial A}{\partial x} + A\frac{\partial V}{\partial x} = 0 \tag{8}$$

$$\frac{\delta U_i}{\delta t_i} + \rho U_i \frac{\partial U_i}{\partial x_i} - \frac{\partial P}{\partial x_i} + \frac{\partial}{\partial x_i}\left(\mu \frac{\partial U_i}{\partial x_j} - \rho u'_j u'_i \right) + \rho g_i \tag{9}$$

where U_i and u'_i are the average velocity and the swing velocity, respectively, in the x_i direction, $x_i = (x, y, z)$, $U_i = (U, V, W)$ and $u'_i = (u', v', w')$. The symbols ρ, μ, P, and g are density, dynamic viscosity, pressure, and gravitational acceleration, respectively. The instantaneous velocity is obtained using the relation $u_i = U_i + u'_i$ for the three Cartesian directions. Simulation in the FLOW-3D model can be done with several turbulence models, including:

1. LES model,
2. k-ω model,
3. k-ε model, and
4. RNG normalized group model.

Table 1 | Numerical and experimental results of the relative energy of the cross-section by comparing different cell sizes

Row	Total cell	ΔE (exp)	ΔE (num)	RE	AE	RMSE
1	454,253	0.54	0.586	14.176	0.073	0.0788
2	577,845	0.54	0.531	5.212	0.034	0.0458
3	858,450	0.54	0.505	0.734	0.008	0.0119
4	920,955	0.54	0.502	0.682	0.008	0.0108

In this research, the RNG model was used. The RNG turbulence model has good performance in simulating flow separation areas and provides better results for the strain and curvature of flow lines. The RNG disturbance model includes two equations, which are presented in Equations (10) and (11), respectively. The reason for using the RNG turbulence model is its ability to simulate a flow with a large computational mesh, good performance in simulating flow separation, superior results with sudden strain and curvature, as well as success in previous numerical studies (Parsaie *et al.* 2016; Simsek *et al.* 2016; Daneshfaraz *et al.* 2020; Ghaderi & Abbasi 2021; Kalateh *et al.* 2024a, 2024b).

$$\frac{\delta U_i}{\delta t_i} + \rho U_i \frac{\partial U_i}{\partial x_i} - \frac{\partial P}{\partial x_i} + \frac{\partial}{\partial x_i}\left(\mu \frac{\partial U_i}{\partial x_j} - \rho u'_j u'_i\right) + \rho g_i u_i \tag{10}$$

$$\frac{\partial}{\partial t}(\rho\varepsilon) + \frac{\partial(\rho\varepsilon u_i)}{\partial x_i} = \frac{\partial}{\partial x_j}\left(\alpha_s \mu_{\text{eff}} \frac{\partial k}{\partial x_j}\right) + C_{1s} - \frac{\varepsilon}{k}(G_k + G_{3s}G_b) + C_{2s} \cdot \rho \frac{\varepsilon^2}{k} - R_\varepsilon + S_\varepsilon \tag{11}$$

2.2. Validation

To validate the numerical data, the study by Daneshfaraz *et al.* (2018) was used, which investigated sudden contraction with three contraction values: 5, 10, and 15 cm. The results are presented in Figure 2. Results show that the numerical data of the present research are in good agreement with the data of Daneshfaraz *et al.* (2018) with the root mean square error coefficient and determination coefficient of 0.046 and 0.97, respectively (Figure 2).

3. RESULTS AND DISCUSSION

3.1. Longitudinal profile and velocity

Figure 3 shows the longitudinal profile of the flow. In this figure, it can be seen that at low flow rates, the flow is submerged. However, as the flow and depth behind the gate increase the flow becomes non-submerged. Results showed that after the flow passes under the gate and along the path, the flow hits the constriction elements, and backflow occurs initially (Figure 4). After the flow reaches the end of the contraction section, the flow leaves the section with a depth lower than the depth of the flow in the desired area and is directed downstream (Figure 4). Figure 4(c) also shows the longitudinal profile of the velocity. It can be concluded that the flow velocity inside the contraction section has decreased due to the increase in the flow depth. This is even though, in addition to increasing the depth of the flow in the desired section, in the empty space between the elements, the depth of the flow has increased near the walls. Figure 4(c) shows the flow velocity in the X-direction. In the submerged flow, the velocity of the flow decreases immediately after passing through the gate, but in the non-submerged flow, the velocity increases until the flow collides with the elements. After the collision with the elements, the depth increases and the velocity decreases. After the flow passes through the narrowed section, the flow continues its path at a higher speed than the narrowed section.

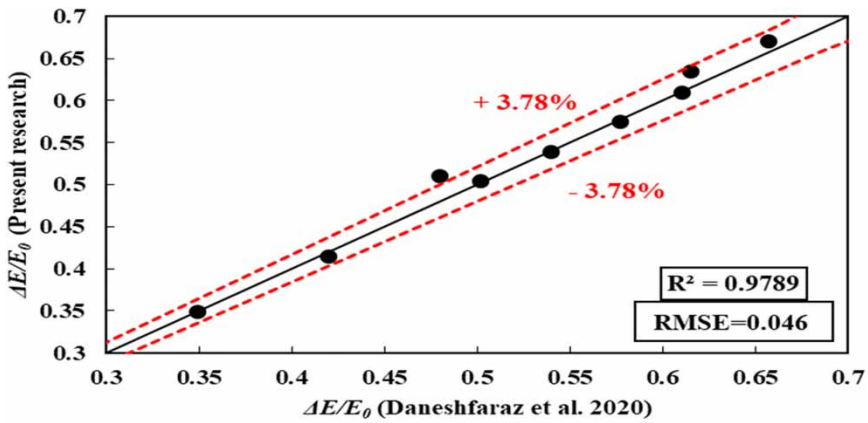

Figure 2 | Validation of the data from the current research with Daneshfaraz *et al.* (2018).

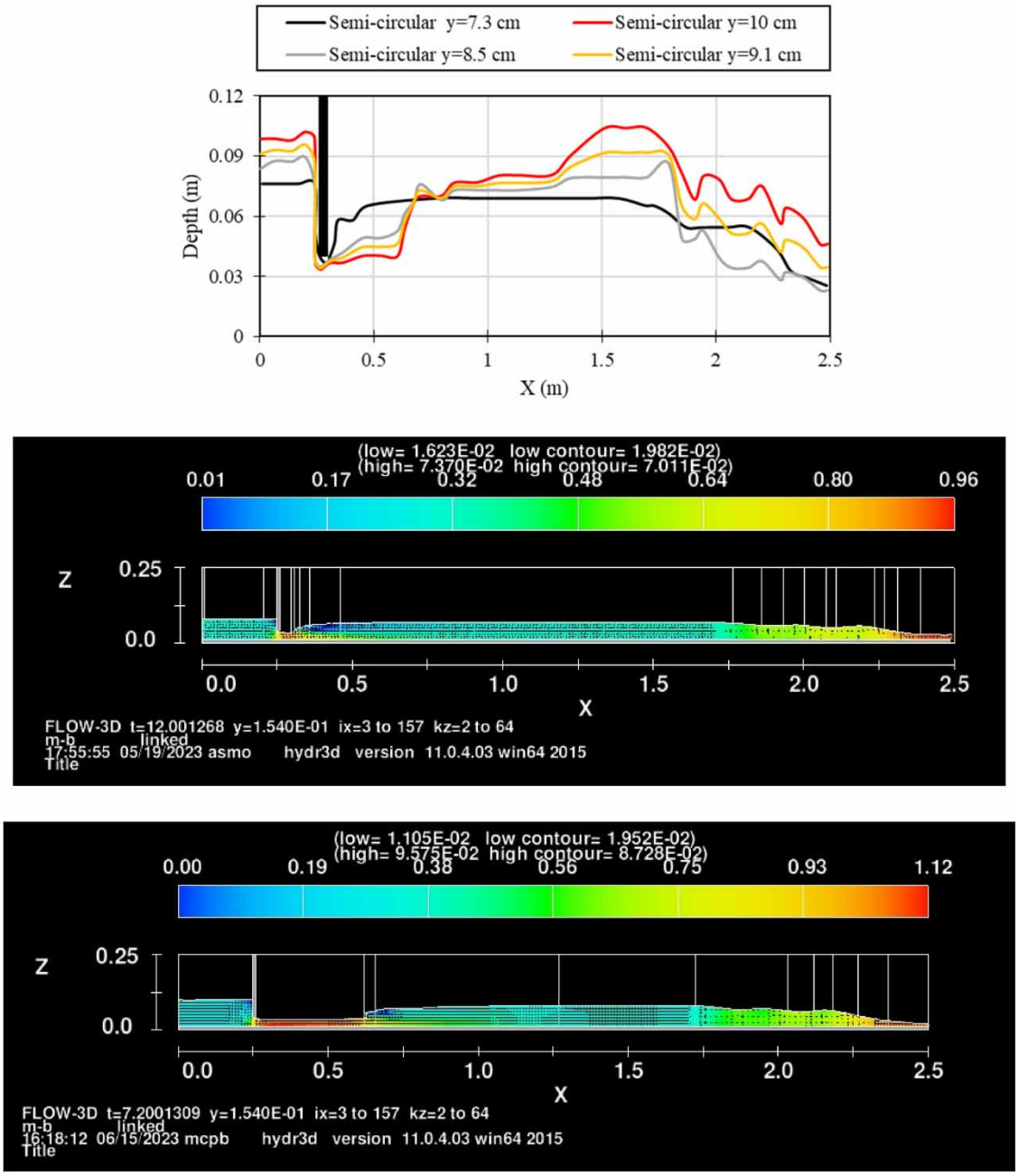

Figure 3 | Longitudinal profiles of flow.

3.2. Energy dissipation

Energy loss for the 10 cm contraction is shown in Figure 5. Figure 5(a) shows the energy loss in the semicircular constriction and Figure 5(b) is related to the energy loss in the trapezoidal constriction. In general, the use of discontinuous constriction causes a greater increase in energy loss. The reason for this is that when the flow impacts the elements, a rip flow occurs, and a portion of the energy loss goes back to the rip flow. On the other hand, some energy loss is related to flow turbulence and losses that occur between gaps in the contraction elements. This effect is larger with semicircular elements than with trapezoidal elements. It was also found that the energy loss in the non-continuous constriction of 10 cm is 39.39% higher than the energy at location A and 62.5% higher than the free hydraulic jump compared with section B.

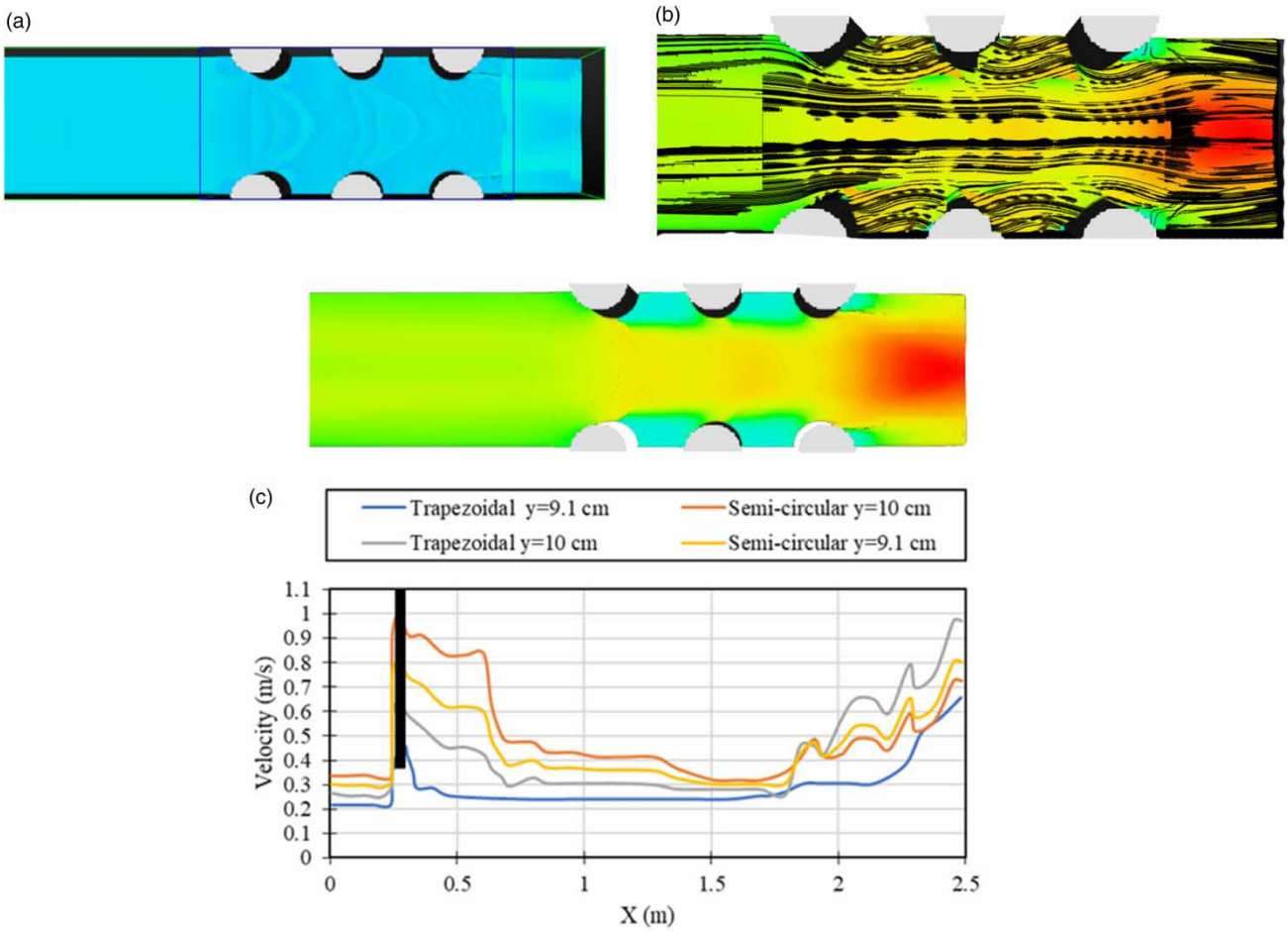

Figure 4 | (a) Longitudinal flow profile; (b) streamlines in a narrowed section; and (c) longitudinal velocity profile.

Similar results are found with the 15 cm contraction. The energy loss changes for the 15 cm contraction can be seen in Figure 6. Results indicate that the energy loss in discontinuous narrowing is greater than that in continuous narrowing. The energy loss in the contraction of 15 cm exceeds that of the 10 cm contraction.

For a contraction of 15 cm, results show that the energy loss is 48.25% higher than the energy in section A and 69.5% higher than the free hydraulic jump compared with section B. Figures 5 and 6 have been prepared to show the changes in fluid energy compared with the energy of the fluid at sections A and B (Figure 5). One of the most important results obtained from the current research is that the narrowness elements have caused an increase in energy dissipation. With the result obtained, it can be suggested that instead of creating stilling basins with large dimensions and high construction costs, the dimensions of the stilling basins should be reduced or removed altogether. This will save a lot of project costs.

With a general and more detailed examination of the obtained results, it was observed that with the narrowing of the channel width, the energy dissipation also increased. This result can somehow indicate that the change in the geometry of the main channel can also play an effective role in the management and design of hydraulic structures.

3.3. Downstream Froude number

Figure 7 shows the changes in the downstream Froude number against the Froude number passing under the gate. In this figure, the changes in downstream Froude number for continuous 10- and 15-cm contractions have been compared with non-continuous contractions of similar sizes.

The results show that as the flow velocity at the inlet increases, the downstream Froude number increases strongly with the constriction elements. The reason for this is that when the streamlines collide with the narrow section, the hydraulic jump

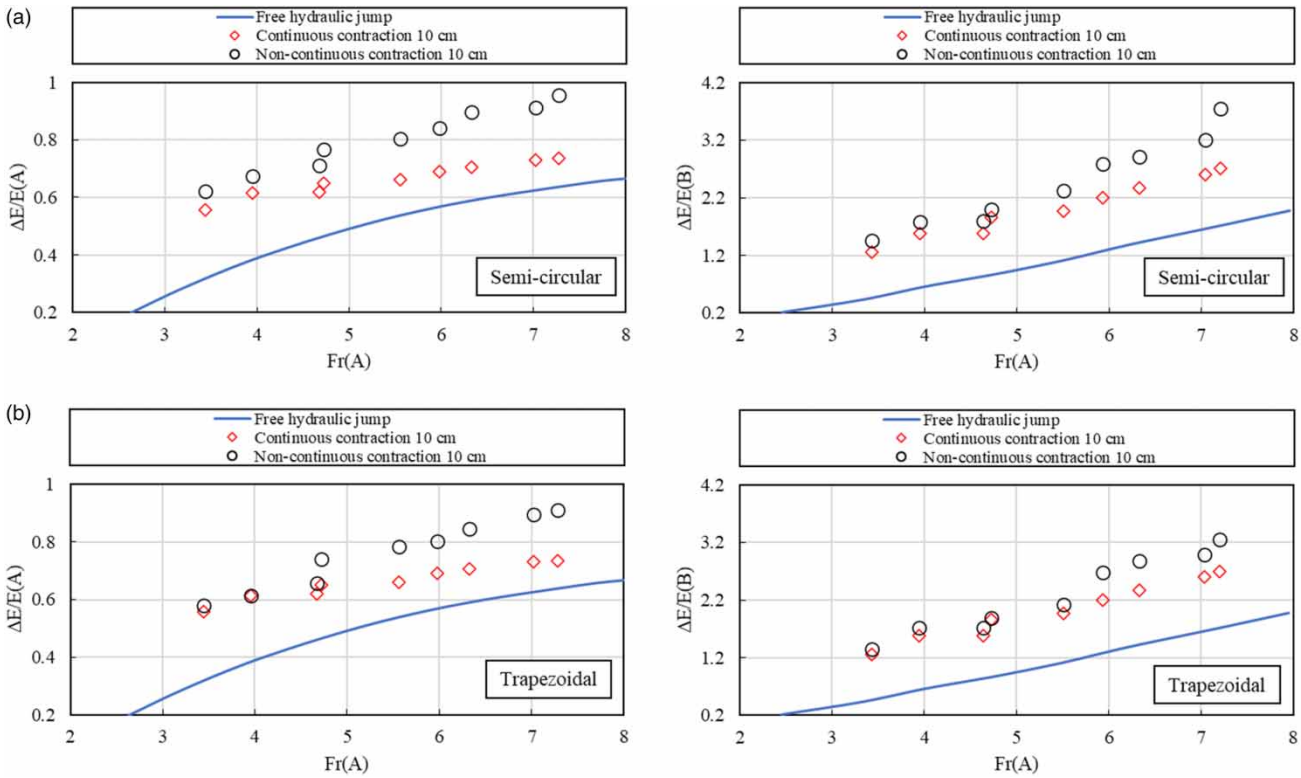

Figure 5 | Relative energy consumption in a 10 cm constriction: (a) semicircular constriction and (b) trapezoidal constriction.

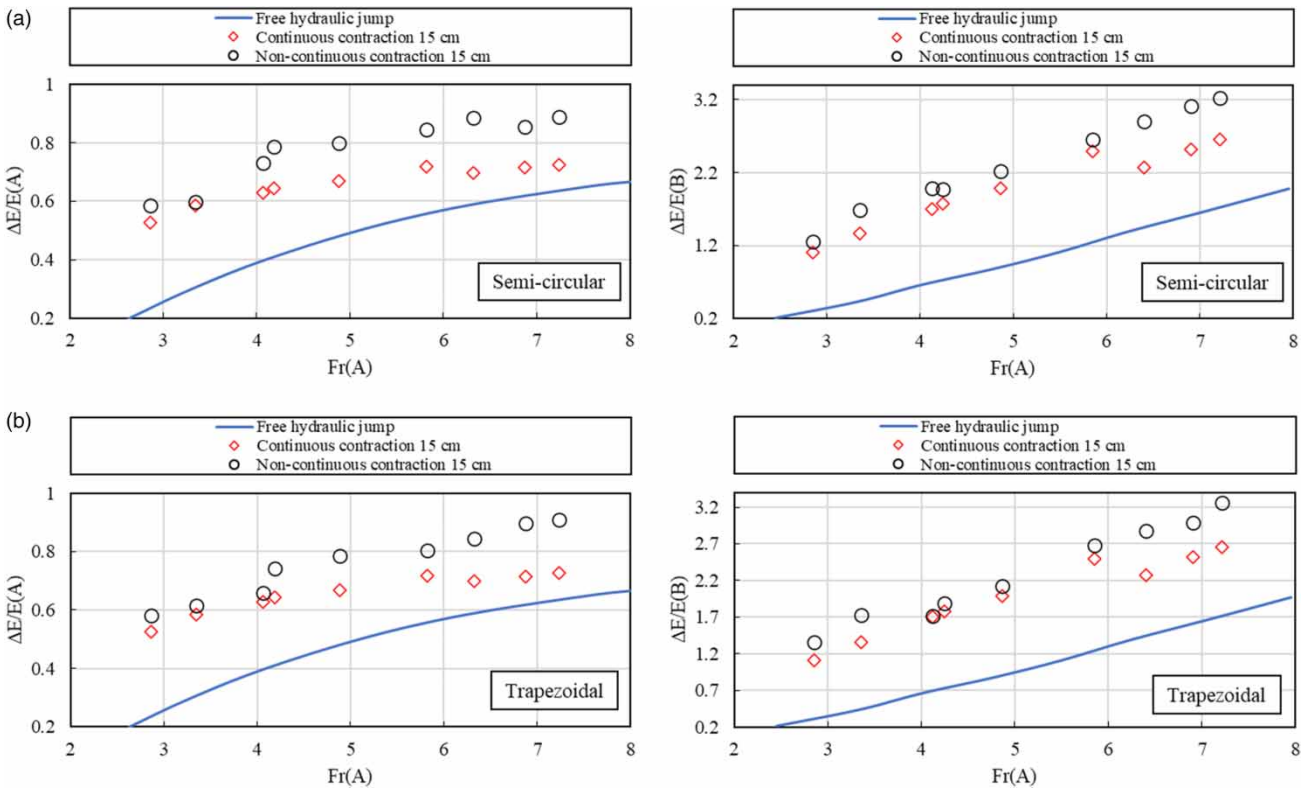

Figure 6 | Relative energy consumption in a 15 cm constriction: (a) semicircular constriction and (b) trapezoidal constriction.

causes an increase in the energy loss, and then, the Froude number in the contraction section decreases. This is even though the Froude number drop compared with the simple case is 68 and 66% for semicircular and trapezoidal constrictions, respectively (Figure 7).

3.4. Downstream depth

The downstream depth parameter is one of the most important parameters that must be considered when using additional elements. The use of supplementary elements has the aim of increasing the depth downstream and reducing the energy of that section.

Figure 8 shows the changes in the relative depth downstream against the energy number passing under the gate (*vena contracta*). Figure 8(a) is related to the semicircular elements and Figure 8(b) is related to the trapezoidal elements. As the flow hits the contraction elements, it causes a further increase in the downstream depth. This has happened both in continuous elements and in non-continuous elements. Results indicated that the increase in flow depth for both continuous and non-continuous elements has similar values, but the maximum relative depth downstream is related to the non-continuous contraction of 15 cm for both semicircular and trapezoidal models (Figure 8).

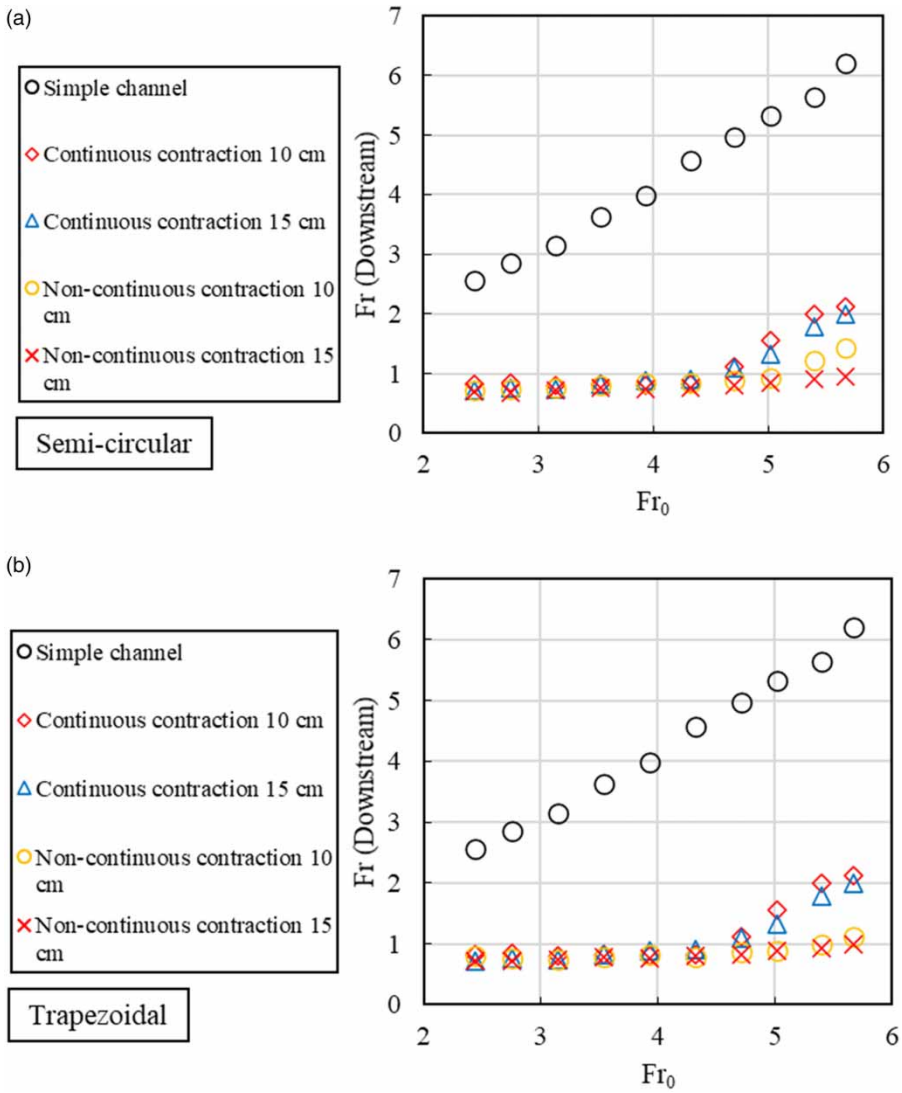

Figure 7 | Variation in the Froude number downstream of (a) semicircular constriction and (b) trapezoidal constriction.

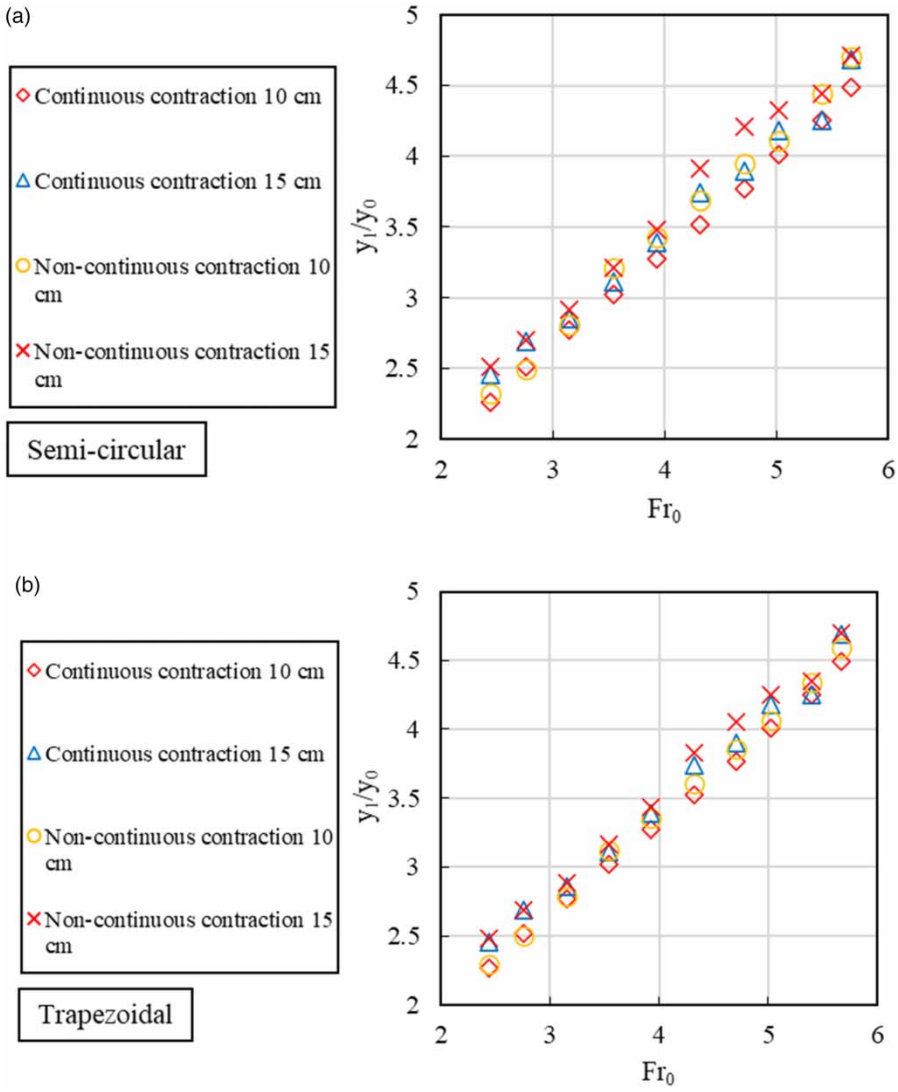

Figure 8 | Changes in the relative depth downstream: (a) semicircular narrowing and (b) trapezoidal narrowing.

4. CONCLUSION

In this research, the effect of sudden non-continuous contraction on the energy dissipation of supercritical flow was numerically investigated. The numerical simulation model was performed with FLOW-3D for two contractions of 10 and 15 cm. Semicircular and trapezoidal geometries were used to create narrowing. The most important results from this research are given below:

1. Investigating the disturbance models indicated that the RNG disturbance model provides superior results compared with other models (Daneshfaraz *et al.* 2018).
2. When the models are compared with each other, the relative energy dissipation increases with the narrowing of the channel width.
3. Some of the energy loss is related to flow turbulence and swirling currents between the gaps in the narrowing elements. The results showed that the energy loss in the non-continuous constriction of 10 cm is 39.39% higher than the energy at location A and 62.5% higher than the free hydraulic jump compared with section B.
4. For a 15 cm narrowing, the results showed that the energy loss compared with section A is 48.25%, and compared with section B, it is 69.5% more than a free hydraulic jump. This value in trapezoidal constriction is 45.73 and 63.6% higher than the free hydraulic jump, respectively.

5. In general, the amount of energy loss in a 15 cm contraction exceeded that of a 10 cm contraction.
6. This result can somehow indicate that the change in the geometry of the main channel can also play an effective role in the management and design of hydraulic structures.

DATA AVAILABILITY STATEMENT

All relevant data are included in the paper or its Supplementary Information.

CONFLICT OF INTEREST

The authors declare there is no conflict.

REFERENCES

Abbaszadeh, H., Daneshfaraz, R. & Norouzi, R. 2023 Experimental investigation of hydraulic jump parameters in sill application mode with various synthesis. *Journal of Hydraulic Structures* **9** (1), 18–42.

Afaridegan, E., Amanian, N., Haghiabi, A., Parsaie, A. & Goodarzi-Mohammadi, A. 2023 Numerical investigation of modified semi-cylindrical weirs. *Water Resources Management* **37** (9), 3715–3728.

Al-Bedyry, N. K., Kadim, M. A., Hussein, S. H., Al-Khafaji, Z. S. & Al-Husseinawi, F. N. 2023 Experimental establishing of moving hydraulic jump in a trapezoidal channel. *Civil Engineering Journal* **9** (4), 873–881.

Chinnarasri, C. & Wongwises, S. 2006 Flow patterns and energy dissipation over various stepped chutes. *Journal of Hydraulic Engineering, ASCE* **116** (4), 587–691.

Daneshfaraz, R., Rezazadeh-Joudi, A. & Sadeghfam, S. 2018 Experimental investigation of energy dissipation in the sudden chocked flow with free surfaces. *Journal of Civil and Environmental Engineering* **48** (2), 101–108.

Daneshfaraz, R., Aminvash, E., Esmaeli, R., Sadeghfam, S. & Abraham, J. 2020 Experimental and numerical investigation for energy dissipation of supercritical flow in sudden contractions. *Journal of Groundwater Science and Engineering* **8** (4), 396–406.

Das, R., Pal, D., Das, S. & Mazumdar, A. 2014 Study of energy dissipation on inclined rectangular contracted chute. *Arabian Journal for Science and Engineering* **39**, 6995–7002.

Ead, S. A. & Rajaratnam, N. 2002 Hydraulic jump on corrugated beds. *Journal of Hydraulic Engineering* **128** (7), 656–663.

Ghaderi, A. & Abbasi, S. 2021 Experimental and numerical study of the effects of geometric appendance elements on energy dissipation over stepped spillway. *Water* **13**, 957.

Hager, W. H. & Dupraz, P. A. 1985 Discharge characteristics of local, discontinuous contractions. *Journal of Hydraulic Research* **23** (5), 421–433.

Harrison, A. J. M. 2015 Design of channels for supercritical flow. *Institution of Civil Engineers* **35**, 475–490.

Hughes, W. C. & Flack, E. J. 1984 Hydraulic jump properties over a rough bed. *Journal of Hydraulic Engineering* **110** (12), 1755–1771.

Izadjoo, F., Shafaei Bajestan, M. & Bina, M. 2005 Hydraulic jump characteristics on a trapezoidal corrugated bed. *The Scientific Journal of Agriculture (SJA)* **27**, 107–122.

Kalateh, F., Aminvash, E. & Abraham, J. 2024a On the effect of flow regime and slope of the channel bed on the hydraulic performance of the sharp-crested rectangular side weir: A numerical simulation. *European Journal of Environmental and Civil Engineering* 1–18.

Kalateh, F., Aminvash, E. & Daneshfaraz, R. 2024b On the hydraulic performance of the inclined drops: The effect of downstream macro-roughness elements. *AQUA – Water Infrastructure, Ecosystems and Society* **73** (3), 553–568.

Kaushik, V. V. R., Ghosh, S., Das, G. & Das, P. K. 2012 CFD simulation of core annular flow through sudden contraction and expansion. *Journal of Petroleum Science and Engineering* **86**, 153–164.

Kyriakopoulos, G. L., Aminpour, Y., Yamini, O. A., Movahedi, A., Mousavi, S. H. & Kavianpour, M. R. 2022 Hydraulic performance of Howell–Bunger and butterfly valves used for bottom outlet in large dams under flood hazards. *Applied Sciences* **12** (21), 10971.

Molinas, A. 2000 *User's Manual for BRI-STARS (Bridge Stream Tube Model for Alluvial River Simulation) (No. FHWA-RD-99-190)*. Federal Highway Administration. Office of Infrastructure Research and Development, USA.

Norouzi, R., Ebadzadeh, P., Sume, V. & Daneshfaraz, R. 2023 Upstream vortices of a sluice gate: An experimental and numerical study. *AQUA – Water Infrastructure, Ecosystems and Society* **72** (10), 1906–1919.

Parsaie, A., Dehdar-Behbahani, S. & Haghiabi, A. H. 2016 Numerical modeling of cavitation on spillway's flip bucket. *Frontiers of Structural and Civil Engineering* **10**, 438–444.

Parsaie, A., Moradinejad, A. & Haghiabi, A. H. 2018 Numerical modeling of flow pattern in spillway approach channel. *Jordan Journal of Civil Engineering* **12** (1), 1–18.

Parsaie, A., Dehdar-Behbahani, S., Devi, G. S. L., Haghiabi, A. & Afaridegan, E. 2023 The discharge coefficient of SMBF flumes under free and submerged conditions. *Applied Water Science* **13** (12), 236.

Samani, Z. A., Baharvand, S. & Davis, S. 2021 Calibration of stage–discharge relationship for rectangular flume with central cylindrical contraction. *Journal of Irrigation and Drainage Engineering* **147** (8), 06021006.

Simsek, O., Akoz, M. S. & Soydan, N. G. 2016 Numerical validation of open channel flow over a curvilinear broad-crested weir. *Progress in Computational Fluid Dynamics, an International Journal* **16** (6), 364–378.

Yamini, O. A., Movahedi, A., Mousavi, S. H., Kavianpour, M. R. & Kyriakopoulos, G. L. 2022 Hydraulic performance of seawater intake system using CFD modeling. *Journal of Marine Science and Engineering* **10** (7), 988.

First received 3 April 2024; accepted in revised form 11 June 2024. Available online 25 June 2024